



## Article

# Entropy Generation in Thermal Radiative Loading of Structures with Distinct Heaters

Mohammad Yaghoub Abdollahzadeh Jamalabadi <sup>1</sup> , Mohammad Reza Safaei <sup>2,3</sup>,  
Abdullah A. A. Alrashed <sup>4</sup>, Truong Khang Nguyen <sup>2,3,\*</sup>  and Enio Pedone Bandarra Filho <sup>5</sup>

<sup>1</sup> Department of Mechanical, Robotics and Energy Engineering, Dongguk University-Seoul, Seoul 04620, Korea; abdollahzadeh@dongguk.edu or muhammad\_yaghoob@yahoo.com

<sup>2</sup> Division of Computational Physics, Institute for Computational Science, Ton Duc Thang University, Ho Chi Minh City 70000, Vietnam; cfd\_safaei@tdt.edu.vn

<sup>3</sup> Faculty of Electrical and Electronics Engineering, Ton Duc Thang University, Ho Chi Minh City 70000, Vietnam

<sup>4</sup> Department of Automotive and Marine Engineering Technology, College of Technological Studies, The Public Authority for Applied Education and Training, Kuwait 130192, Kuwait; aaa.alrashed@yahoo.com

<sup>5</sup> School of Mechanical Engineering, Federal University of Uberlandia (UFU), Av. Joao Naves de Avila, 2121, Santa Monica, Uberlandia MG 38408-514, Brazil; bandarra@ufu.br

\* Correspondence: nguyentruongkhang@tdt.edu.vn

Received: 20 July 2017; Accepted: 18 September 2017; Published: 29 September 2017

**Abstract:** Thermal loading by radiant heaters is used in building heating and hot structure design applications. In this research, characteristics of the thermal radiative heating of an enclosure by a distinct heater are investigated from the second law of thermodynamics point of view. The governing equations of conservation of mass, momentum, and energy (fluid and solid) are solved by the finite volume method and the semi-implicit method for pressure linked equations (SIMPLE) algorithm. Radiant heaters are modeled by constant heat flux elements, and the lower wall is held at a constant temperature while the other boundaries are adiabatic. The thermal conductivity and viscosity of the fluid are temperature-dependent, which leads to complex partial differential equations with nonlinear coefficients. The parameter study is done based on the amount of thermal load (presented by heating number) as well as geometrical configuration parameters, such as the aspect ratio of the enclosure and the radiant heater number. The results present the effect of thermal and geometrical parameters on entropy generation and the distribution field. Furthermore, the effect of thermal radiative heating on both of the components of entropy generation (viscous dissipation and heat dissipation) is investigated.

**Keywords:** thermal radiation; natural convection; entropy generation; thermal loading

## 1. Introduction

The shortage of fossil fuel energy sources, energy costs in industry, the growth of energy demand, and the sustainable use of energy necessitate the an increase in the amount and quality of energy sources. Energy balance analysis, energy quality evaluation, recovery, and utilization, and environmental and energy saving opportunities from the perspective of the thermodynamic happens in many applications, such as heat generated within thermal plasma processing in a vacuum [1], the optimal design of a thermal loading furnace [2], thermal loading systems [3], biomass and biofuels, for instance the unburnt carbon for a coal-fired utility boiler [4], compressible fluid flow [5], entropy generation in heat exchangers [6], energy collected/derived from natural processes, for instance ocean currents and sea wave energy converters [7], renewable energy, for instance wind turbine blades [8], forced and natural convective boiling [9–11], heat transfer in a micro channel [12,13], porous media [14], closed conduits [15], and spark ignition engines [16].

From the view point of scientific and engineering applications, Jamalabadi et al. [17] initiated the study on conjugate heat and fluid flow in a discrete heat source thermal radiative loading of a thin plate's boundary layer flow. Jamalabadi et al.'s work was advanced in efficient numerical modeling [18], temperature-dependent effects of thermal properties [19], three-dimensional simulations and stability analysis for convection induced by an absorption of radiation [20], and combustion optimization [21].

Earlier, the goal was to reach the required heat capacity and heat transfer rate with the highest obtainable efficiency. Later, the economic aspects (minimum production and repair cost) became essential to energy strategies. There are many optimization procedures to find the optimum design between possible cases. One method is based on the second law of thermodynamics or entropy generation minimization (EGM). Entropy generation effects in thermal loading and furnace applications have not been discussed yet, although a number of studies have reflected the second law analysis of thermodynamics in enclosure heating applications [22–30]. In the special case of radiant heating, radiative convection heat transfer and natural convection play a significant role. The role of geometrical parameters, such as different shapes, sizes, and number of solar heaters [22], circular corners [23], and inner cylinders [24] for entropy generation studies in square and triangular cavities during natural convection have been discussed recently. The various process fluids' properties (nano-fluids, non-Newtonian, micro polar) also affect the entropy generation of natural convection circulation in containers/enclosures [25–34].

A comprehensive and detailed review of irreversibility measured by entropy generation versus energy efficiency during natural convection-based energy flow in enclosures (of various shapes, such as rectangular, trapezoidal, triangular, rhombic, and wavy) and processes is done by Biswal and Basak [35]. The entropy generation of natural convection of open enclosures in three-dimensions is studied by Oztop et al. [36], where the opening ratio, center of opening, and Rayleigh number were the key parameters. They proved that the edge of an opening is the dominant parameter where the highest heat transfer and entropy generation is for the fully opened cavity. Hussain et al. [37] considered some obstacles in their open cavity and studied the entropy generation. An adiabatic obstacle acts as a delaying body to the flow, and when the flow touches the obstacle, it circumvents the obstacle by passing above and below it. The obstacle's position affects the fluid amount that enters into the cavity and hence changes the amount of entropy generation. Furthermore, the role of surface thermal radiation on entropy generation in an open cavity with natural convection is studied by Hinojosa et al. [38]. The results of Hinojosa et al. [38] point out that thermal radiation of a surface increases the overall entropy generation rate (33.52–560.87%), and cannot be neglected in the analysis of open cavity entropy generation.

Considering all the above, the current paper aims at the study of entropy production in a steady state natural convection of air flow in a thermal-loaded enclosure where the loaded wall is adiabatic and the other wall is subjected to constant wall temperatures. The effects of thermal radiation, geometrical parameters, and thermal loading parameters on entropy generation are studied numerically. The results of the study are presented by entropy field contours and 2D plots of entropy generation and Bejan numbers as a function of system parameters.

## 2. Mathematical Modeling

To study the thermodynamics aspects of radiant loading, a system consisting of distinct heaters in an open cavity (outlet at the medium temperature  $T_\infty$ ) filled by air in a laminar fluid flow regime, where the bottom surface plate is cooled at a constant temperature ( $T_c$ ) and the upper non-permeable sheet is heat loss prohibited (adiabatic), as given by the Cartesian two-dimensional (2D) (an infinitely large medium is assumed in the third direction) sketch shown in Figure 1, is considered. The air is assumed to be a Newtonian and compressible fluid with a temperature-dependent viscosity.

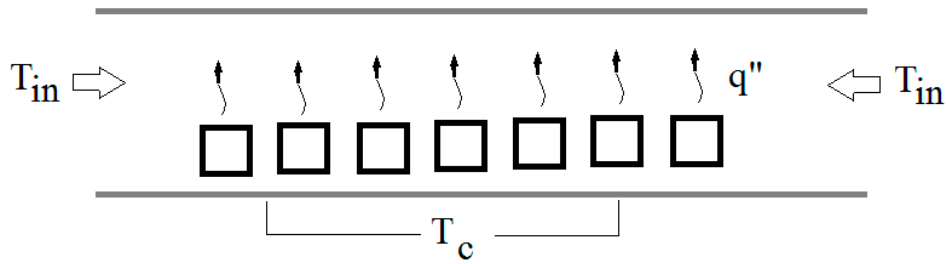


Figure 1. Schematic representation of the problem.

As shown in the 2D presentation of the system in Figure 1, the radiant discrete heaters are placed at a constant distance from the bottom plate to heat the top plate by a thermal radiation heat transfer mode. The bottom plate is needed to confine the cavity, sustain the electrical connection of the heaters, and provide structural support to both ends of the heaters in the third dimension (normal to the page direction). The bottom plate also should be kept at a constant temperature ( $T_c$ ) to maintain the electrical connections in the safe and allowable range. As the working fluid here (air) is compressible, the cavity is not completely closed to avoid the rupture and bursting of the system. Bursting can occur because of the increase of working fluid volume as it heats. The other benefit of the open cavity is to let the emergency system cool the heaters, electrical wires, and materials in case of melting or fire. The input heat to the system (which appeared as heat flux in discrete sources in the radiant heating of the top plate) is usually high enough to induce natural convection.

In Cartesian coordinates, the continuity equation of the fluid is:

$$\nabla \cdot (\rho \vec{v}) = 0 \quad (1)$$

where  $\vec{v}$  is the velocity vector with components of  $(u, v)$  in the  $(x, y)$  directions. The set of equations that describe fluid momentum conservation are the Navier–Stokes equations. In Cartesian coordinates, the Navier–Stokes equations are:

$$(\vec{v} \cdot \nabla) \vec{v} + \frac{\nabla p}{\rho} + g[1 - \alpha(T - T_0)] \vec{i}_y = \nu \nabla^2 \vec{v} \quad (2)$$

where  $(u, v)$  are the velocity components in the  $(x, y)$  directions, respectively, and  $\rho$  is the fluid density. The external gravity field is in the  $(-y)$  direction it where produces natural flow in the fluid near the discrete heat sources and all over the enclosure. The Newtonian model is used here for modeling the viscosity, and the viscosity is modeled by the ideal gas with the molecular mass of 28.97 (g/mol).

The energy equation of fluid flow, which is not affected by thermal radiative absorbance (the medium is assumed to be transparent for thermal radiation), is:

$$\rho c_p (\vec{v} \cdot \nabla) T = -\nabla \cdot \vec{q} + \bar{\tau} : \nabla \vec{v}. \quad (3)$$

The first term is accumulation of energy through convection, the second is the heat flux diffusion, and the last is energy dissipation release per unit volume. The fluid considered here is assumed to have no interaction with thermal radiation, such as absorption, scattering, and extinction. Since the effect of thermal radiation is restricted to the surface, the surface radiation within the cavity is:

$$\sum (\delta_{ij} - F_{ij}) \sigma_B T^4 = \sum (\delta_{ij} - (1 - \varepsilon_j) F_{ij}) \frac{q''_j}{\varepsilon_j}. \quad (4)$$

The thermal radiation effect on entropy generation here is done indirectly by the heating surface and natural convection inducement. The input energy to the system from the discrete heat sources

is used to heat the top plate, dissipate through the cooled bottom wall, and interact with the environmental temperature ( $T_\infty$ ). The related velocity boundary conditions at the solid walls are:

$$\vec{v} = 0. \quad (5)$$

A similar thermal boundary condition to that reported by Abdollahzadeh et al. [17] is considered to study the effect of discrete sources radiant heating. The input flux is assumed to be applied uniformly from the surface of the discrete heat sources to the fluid, as

$$\frac{\partial T}{\partial n} = \frac{-q''}{k_f} \quad (6)$$

where  $n$  is the normal to the surface direction, and the other boundaries are at

$$\frac{1}{2} \rho \vec{v}^2 (x = L/2) + p(x = L/2) = p_\infty \quad (7)$$

$$u(x = 0) = 0 \quad (8)$$

$$T(y = 0) = T_w \quad (9)$$

$$\frac{\partial T}{\partial x}(x = 0) = 0 \quad (10)$$

$$T\left(x = \frac{L}{2}\right) = T_\infty. \quad (11)$$

The system of nonlinear governing equations is non-dimensionalized based on the non-dimension parameters that are given in the nomenclature. Following are the non-dimensional main conservative equations of mass, momentum, fluid energy, and solid energy:

$$\frac{\partial U}{\partial X} + \frac{\partial V}{\partial Y} = 0 \quad (12)$$

$$U \frac{\partial U}{\partial X} + V \frac{\partial U}{\partial Y} = \frac{-\partial P}{\partial X} + \text{Pr} \nabla^2 U \quad (13)$$

$$U \frac{\partial V}{\partial X} + V \frac{\partial V}{\partial Y} = \frac{-\partial P}{\partial Y} + \text{Pr} \nabla^2 V + \text{Ra} \text{Pr} \theta \quad (14)$$

$$U \frac{\partial \theta}{\partial X} + V \frac{\partial \theta}{\partial Y} = \nabla^2 \theta \quad (15)$$

$$\sum_{j=1}^n (\delta_{ij} - F_{ij}) \Theta_j^4 = \sum_{j=1}^n (\delta_{ij} - (1 - \varepsilon_j) F_{ij}) \frac{q''_j}{\varepsilon_j} \quad (16)$$

with the non-dimensionalized boundary condition of  
at  $Y = 0$ :

$$U = V = 0, \frac{\partial P}{\partial y} = 0, \Theta = 1 \quad (17)$$

at  $Y = A$ :

$$U = V = 0, \frac{\partial P}{\partial Y} = 0, \frac{\partial \Theta}{\partial Y} = 0 \quad (18)$$

at heaters:

$$U = V = 0, \frac{\partial P}{\partial n} = 0, q'' = -k \frac{\partial T}{\partial n} \quad (19)$$

at  $X = 0$ :

$$\frac{\partial P}{\partial X} = 0, U = 0, \frac{\partial \Theta}{\partial X} = 0, \frac{\partial V}{\partial X} = 0 \quad (20)$$

at  $X = 1$ :

$$P = P_{\infty} - \rho u_{in}^2, \frac{\partial V}{\partial X} = 0, \frac{\partial U}{\partial X} = -\frac{\partial V}{\partial Y}, \Theta = 1 \text{ if } U < 0, \frac{\partial \Theta}{\partial X} = 0 \text{ if } U \geq 0. \quad (21)$$

The entropy definition for the fluid is taken from:

$$S = C_p(T) \ln\left(\frac{T}{T_{\infty}}\right) - R \ln\left(\frac{\rho}{\rho_{\infty}}\right). \quad (22)$$

The irreversibility in the convective fluid flow has the two components of energy and momentum. Consequently, local volumetric entropy production may occur as a result of fluid friction and heat transfer in the direction of the finite temperature gradients. The volumetric rate of entropy generation is given by:

$$S'''_g = \frac{1}{T^2} k_f \left[ \left( \frac{\partial T}{\partial x} \right)^2 + \left( \frac{\partial T}{\partial y} \right)^2 \right] + \frac{\mu}{T} \left[ 2 \left( \frac{\partial u}{\partial x} \right)^2 + 2 \left( \frac{\partial v}{\partial y} \right)^2 + \left( \frac{\partial u}{\partial y} + \frac{\partial v}{\partial x} \right)^2 \right]. \quad (23)$$

The first term in Equation (23) refers to the heat transfer irreversibility and the second term symbolizes the local entropy generation rate due to fluid friction. The second term is presented in some references as the viscous dissipation function and is represented by  $\Phi$  [14]. The total entropy generation is usually non-dimensionalized by  $k_f/L^2$ , and presented by the entropy generation number ( $N_s$ ). In order to clarify the physical principle, in this paper, non-dimensionalized parameters such as the Bejan number are used from the literature to measure the proportion of heat transfer irreversibility (first term in Equation (23)) in total irreversibility and is defined by [29,30]:

$$Be = \frac{\frac{1}{T^2} k_f \left[ \left( \frac{\partial T}{\partial x} \right)^2 + \left( \frac{\partial T}{\partial y} \right)^2 \right]}{\frac{1}{T^2} k_f \left[ \left( \frac{\partial T}{\partial x} \right)^2 + \left( \frac{\partial T}{\partial y} \right)^2 \right] + \frac{\mu}{T} \left[ 2 \left( \frac{\partial u}{\partial x} \right)^2 + 2 \left( \frac{\partial v}{\partial y} \right)^2 + \left( \frac{\partial u}{\partial y} + \frac{\partial v}{\partial x} \right)^2 \right]}. \quad (24)$$

### 3. Results and Discussion

Based on the semi-implicit method for pressure linked equations (SIMPLE) finite volume method, a method was developed to solve the coupled radiation and natural convection problem in a cavity, and the method was verified by the well-known benchmarks shown in Table 1. The systems of Equations (12)–(21), over the domain presented in Figure 1, are solved numerically. In order to have an insight into the problem, an in-house FORTRAN code was written to compute and generate the contour graphs for the velocity, temperature, and entropy generation rate for different values of the governing parameters in order to be able to comment on their importance in the entropy generation. The produced uniform grid spaces ( $\Delta X = \Delta Y$ ) are examined versus the convergence of the Nusselt number and maximum stream function in Table 2 for constant grid sizes over the domain between 0.1 and 0.005. As presented in Table 2 for the grid independence test, finally the grid size of  $\Delta X = \Delta Y = 0.01$  is chosen such that the change in Nusselt number for the maximum and minimum grid sizes is about 0.02%.

**Table 1.** Verification study with the benchmarks.

| Ra     | Nu                  |                    |               |
|--------|---------------------|--------------------|---------------|
|        | Dixit and Babu [32] | de Vahl Davis [33] | Current Study |
| $10^3$ | 1.120               | 1.116              | 1.13          |
| $10^4$ | 2.286               | 2.242              | 2.25          |
| $10^5$ | 4.563               | 4.531              | 4.54          |
| $10^6$ | 8.800               | 9.035              | 8.9           |

**Table 2.** Grid convergence study at  $N = 11$  and  $N_r = 55.31$  for square cavity.

| $\Delta X$ | $Nu$  | %      | $\Psi_{max}$ | %      |
|------------|-------|--------|--------------|--------|
| 0.1        | 53.12 | 9.5522 | 285.46       | 2.3668 |
| 0.05       | 57.37 | 2.3157 | 274.93       | 1.4093 |
| 0.01       | 58.72 | 0.0170 | 280.15       | 0.4626 |
| 0.005      | 58.73 | 0.0    | 278.86       | 0.0    |

The results of three lamps with  $N_r = 10$  and  $A_R = 1/2$  are shown in Figure 2. As shown, the contours of the dimensionless temperature field were distributed uniformly around the heat sources, and their value decreased by an increase of distance from the discrete heat sources. The dimensionless quantities of  $N_r = 10$  and  $A_R = 1/2$  are selected arbitrarily to study the effect of the parameters on the system's behavior. The value of the Prandtl number is used here and is adapted with the value of air ( $Pr = 0.71$ ). The thermal radiation heating leads to high temperature zones from just around the discrete heat sources to the whole cavity. Even though the isotherms are modified by the velocity field (from the stratified case of pure heat conduction), the general entropy generation trend is dominated by the heated part. The natural convection helps the cooling via the cavity, but the general configuration of the temperature field is not affected by the fluid flow.

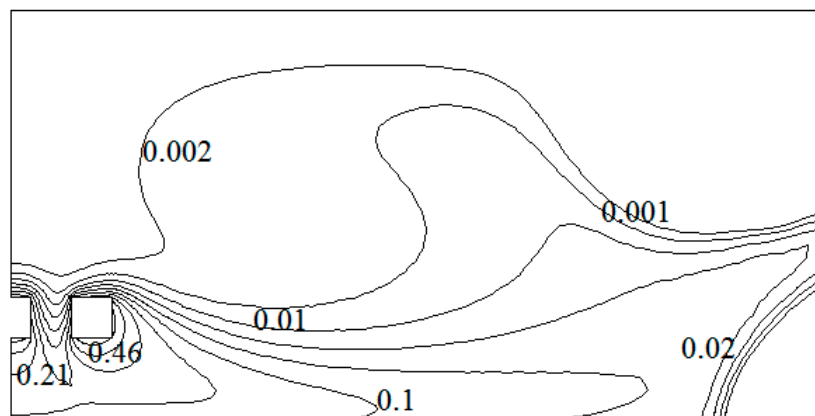
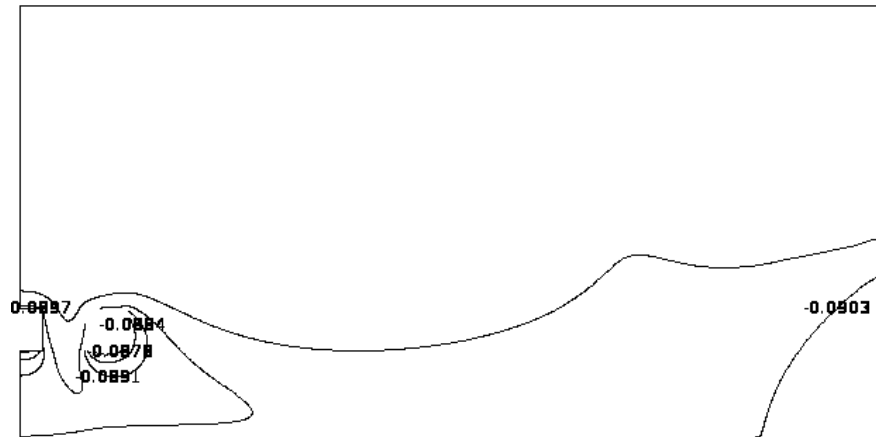
**Figure 2.** Dimensionless temperature contours for three discrete heat sources with  $N_r = 10$  and  $A_R = 1/2$ .

Figure 3 depicts the non-dimensionalized entropy distribution based on the definition of Equation (22) for the same values of parameters used in Figure 2. The entropy value was non-dimensionalized by the  $C_p$  value, and presents a similar behavior to Figure 3, as the entropy amount was most influenced by temperature rather than density. The maximum values of entropy occur near the discrete heat sources, while the minimum values take place near the outlet and near the top adiabatic plate. A comparison of the heating patterns (Figure 2) and entropy generation (Figure 3) within the open cavity involving the discrete heat sources shows similar trends. The augmentation of entropy generation close to the discrete heat sources at the middle of the cavity (near the symmetry line) and the strong section in the bottom part of the cavity is strengthened by the heat transfer.

The local entropy generation rate due to the heat component is depicted in Figure 4. As revealed in Figure 4, most of the entropy generated by heat transfer is concentrated near the thermal boundary layer of the discrete heat sources. Although the rate of heat component of the entropy generation is highest near the discrete heat sources, it decreases suddenly as the distance from the discrete heat sources increased. As a result of the discrete source heating, the heat transfer is larger at the surfaces of the discrete heat sources; thus, the rate of heat component of the local entropy generation due to heat transfer is significant at those points rather than at the top plate and left portion of the bottom plate, and a high entropy generation zone spreads and augments substantially. The heat transfer irreversibility

at the central zone is insignificant due to the almost uniform temperature distribution. The velocity contours are clustered at the outlet of the open cavity, and the local fluid friction irreversibility is larger at those zones. At the middle of the cavity, as the conductive heat transfer mode dominates over the convective heat transfer mode, the entropy generation is mainly due to convective heat transfer.



**Figure 3.** Dimensionless entropy contours for three discrete heat sources with  $Nr = 10$  and  $A_R = 1/2$ .

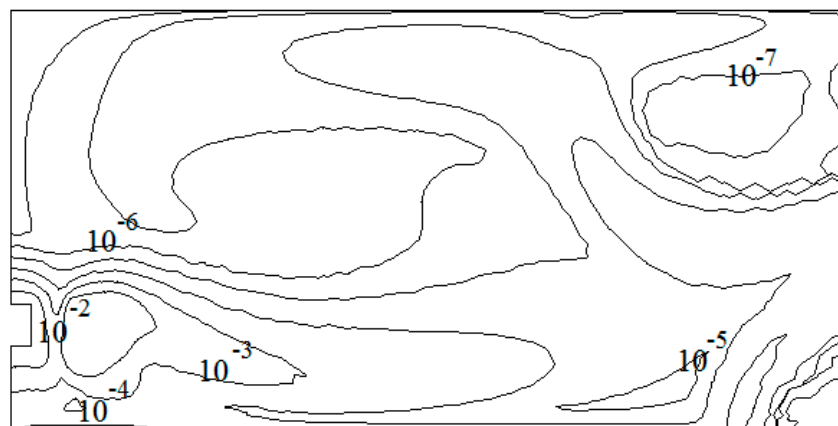


**Figure 4.** Dimensionless rate of heat component of entropy generation for three discrete heat sources with  $Nr = 10$  and  $A_R = 1/2$ .

Figure 5 presents the contours of the dimensionless rate of fluid flow induced component of entropy generation for three discrete heat sources with  $Nr = 10$  and  $A_R = 1/2$ . The values of the rate of fluid flow induced component of entropy generation are non-dimensionalized by the  $k_f/L^2$ , in the same way as done in Figure 4, to make a complete comparison. As shown, due to larger velocity gradients, the maximum of fluid flow induced entropy generation occurred in the right edge of the top plate. As the fluid enters from the bottom to the cavity and warms up though it (upswings alongside the symmetry of cavity), it accelerates by natural convection, and finally exits the cavity by the uppermost velocity at the top of the cavity as shown in other references [17,18]. Since the uppermost velocity's interaction with the top plate boundary causes the highest value of vorticity and viscous dissipation at that place, the most powerful dissipation happens at the turning streamlines at the outlet boundaries of the cavity.



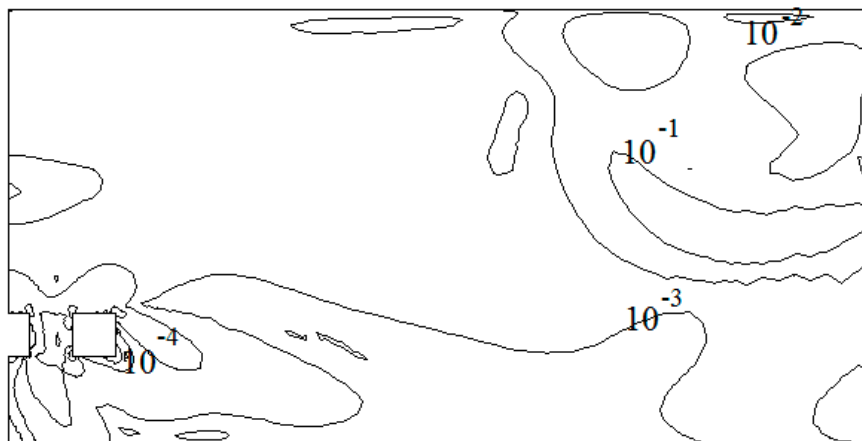


**Figure 5.** Dimensionless rate of friction component of entropy generation for three discrete heat sources with  $N_r = 10$  and  $A_R = 1/2$ .

Figure 6 shows the distribution of the dimensionless total rate of entropy generation (by  $k_f/L^2$ ) for three discrete heat sources with  $N_r = 10$  and  $A_R = 1/2$ . As shown, two zones are important in this figure. The first is the zone around the lamps, which contains the maximum values of entropy generation, and the second is the zone at the inlet/outlet of the cavity (open boundary at  $X = 1$ ). Although the interaction of the outlet and top plate (the zone expected to have the maximum value of generated entropy) has the maximum value of friction entropy generated amount, the contribution of the heating part is negligible in this zone, while the zone near the discrete heat sources that has the maximum value of heating entropy generated amount (which is less than the maximum value of friction entropy generated) also benefits from the fluid vortices' dissipation energy caused by the fluid–solid interaction, and finally produces the maximum value of the generated entropy. The distribution of the entropy in the middle of the cavity (on the symmetry line above the discrete heat sources) shows that the entropy generation becomes negligible in that region as a result of the lowest temperature gradient in that region, and no fluid–solid interaction for the vortex-generated entropy contribution.

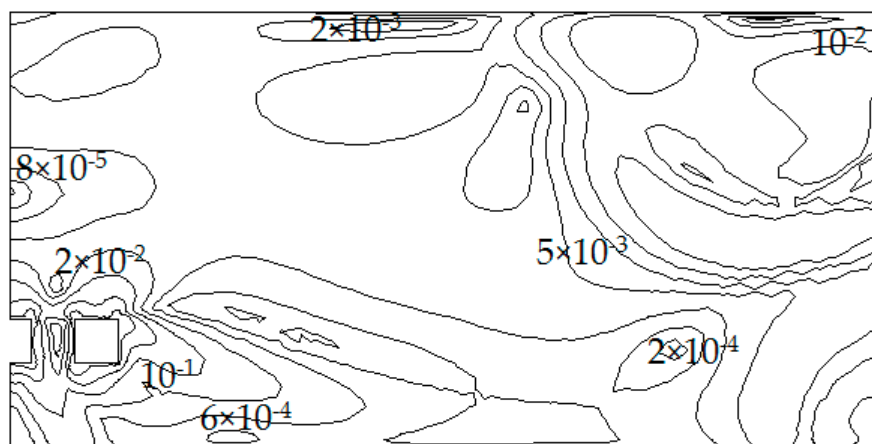


**Figure 6.** Dimensionless rate of total entropy generation for three discrete heat sources with  $N_r = 10$  and  $A_R = 1/2$ .

The adoption and development of entropy generation study in various applications of typical thermal engineering can be evaluated by a study using the Bejan number (an irreversibility distribution parameter defined in Equation (24)). Figure 7 provides an evaluation of the local entropy generation due to heat transfer fluid friction and heat transfer, and the summation of entropy generation, by



presenting the local Bejan number all over the domain. In Figure 7, contours of the local Bejan number, which is calculated at each node on the domain (locally), are illustrated to have a better comparison between the heat and friction part of the generated entropy. As shown in most of the cavity, the Bejan number is less than 0.1. As the local Bejan number represents the dominance of the heat transfer irreversibility, it could be interpreted as the dominance of fluid irreversibility over the domain. Note that  $Be > 0.5$  characterizes principal heat transfer entropy generation inside the open cavity, and alternatively,  $Be < 0.5$  signifies the fluid friction entropy generation governance. Additionally, it shows that, besides the radiant heating nature of this heating, the entropy generation caused by the friction is not negligible. In fact, the local Bejan number contours' density at the lower part of the enclosure confirms that a friction irreversibility pattern exists at the top of the open cavity.

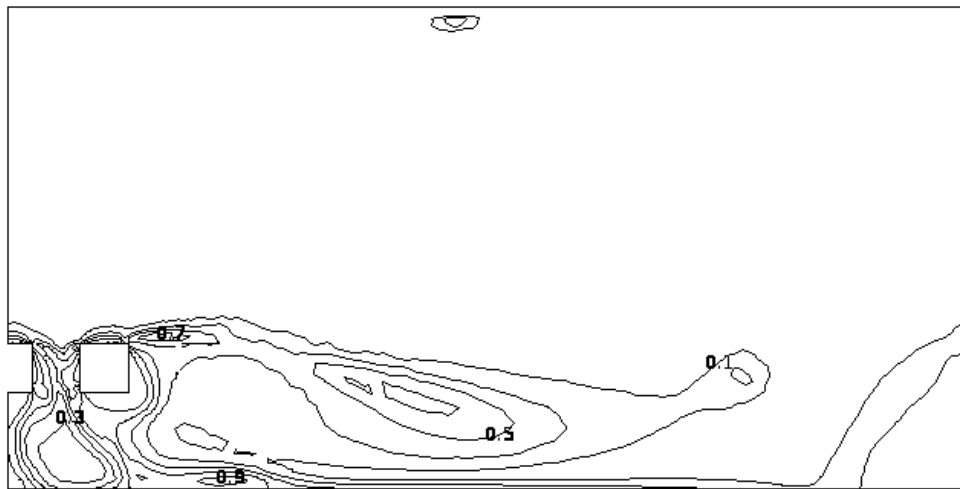
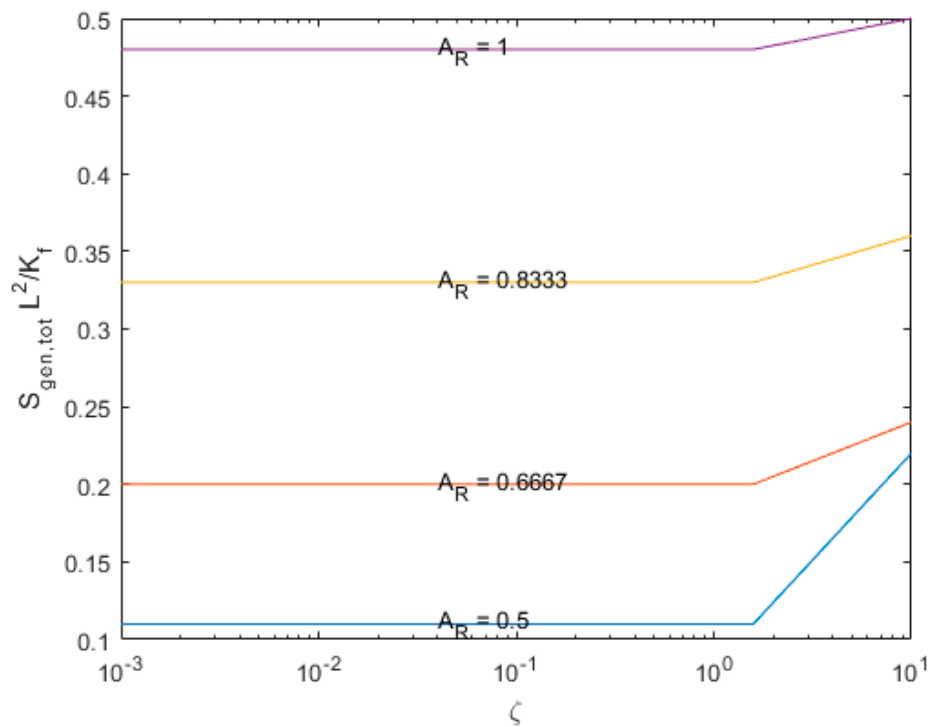


Figure 7. Bejan number for three discrete heat sources with  $Nr = 10$  and  $A_R = 1/2$ .

In addition, most of the heating part of the entropy was generated at the lower side of the cavity with the height less than the locations of discrete heat sources. As shown, the most values of Bejan numbers happen around the heat sources and near the bottom walls. In some studies, the concept of irreversibility distribution ratio (a non-dimensional quantity which is the ratio between the fluid friction irreversibility and heat transfer irreversibility) is used. However, as shown in Figure 7, the range of the Bejan numbers is from 0 to 1, so the authors have not used that term (i.e., irreversibility distribution ratio) here to avoid exposing the zero and infinity irreversibility ratio and the difficulty in choosing the contour level for presentation.

Figure 8 reveals the variation of total entropy generation rate per volume at the open cavity which is calculated globally (during the course of the domain). Generally, it is observable that  $S_{total}$  increases with  $\zeta$  for  $\zeta > 1$  significantly while for  $\zeta < 1$  the changes are negligible. As shown by the increase of heating ratio, the dimensionless entropy generation value in the open cavity remains constant at a low heating number and increases by an increase of heating number. A keen observation of the Figure 8 shows that with the increase of the aspect ratio the dimensionless entropy generation rate per volume increases. The rate of increase of  $S_{total}$  along with the magnitude of  $S_{total}$  are found to be the biggest for  $\zeta = 10$  for all the cases of the aspect ratios.

In addition, the entropy generation has a transition point of  $\zeta = 1$  (for all aspect ratios), which shows a greater contribution of the natural convection heat transfer mode and the thermal radiation heat transfer mode in entropy generation. At the limit of  $\zeta \ll 1$ , the dominant mode of heat transfer is heat conduction. Because the momentum equation is coupled to the fluid energy equation, an increase of the contribution of the natural convection heat transfer mode and the thermal radiation heat transfer mode in the heat transfer causes a greater contribution of fluid flow and entropy generation due to fluid friction, while the total value of the entropy generation also confirms the pattern clearly.

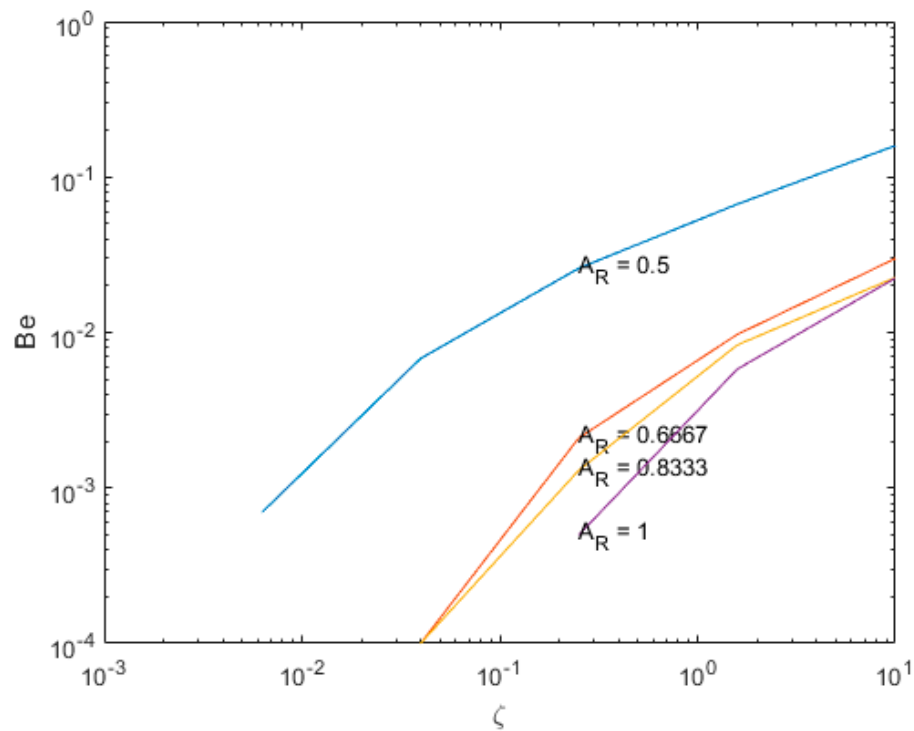


**Figure 8.** Dimensionless rate of total entropy generation for singular discrete heat sources as a function of heating ratio for various aspect ratios.

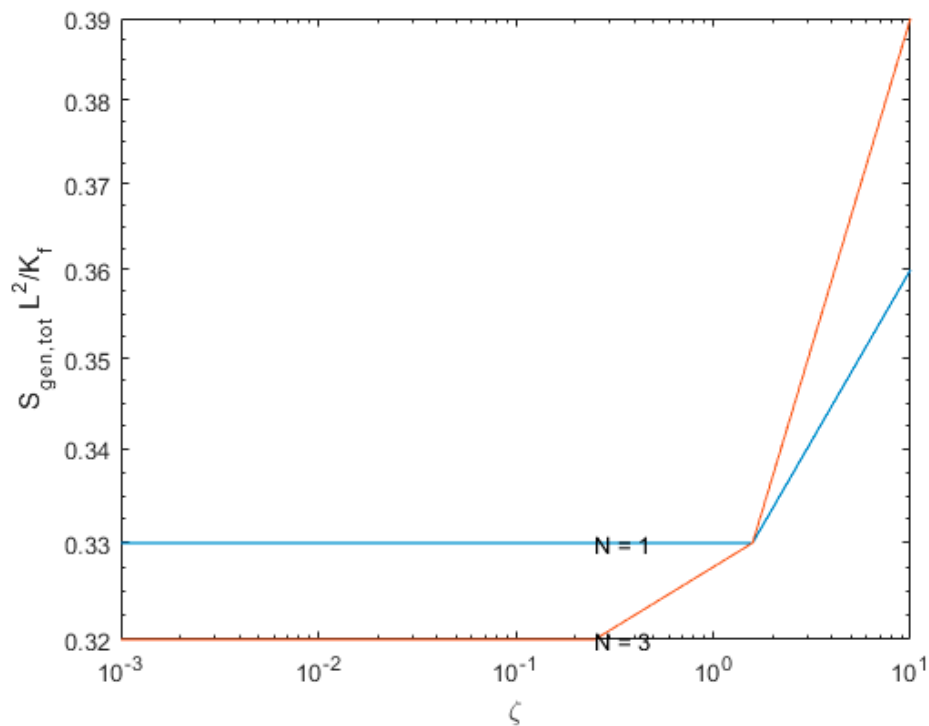
Figure 9 presents considerable variation of Bejan numbers for singular discrete heat sources plotted against heating ratio for a number of aspect ratios inside the open cavity. It is clear from both Figures 8 and 9 that the heating portion of entropy generation in the cavity increases with heating number. Equation (24) clarifies that the contribution of entropy generation due to the heat transfer has a direct relationship with the gradients of isotherms, which is related to the input heat power to the system. Note that  $Be > 0.5$  characterizes principal heat and mass transfer entropy generation inside the open cavity, and alternatively,  $Be < 0.5$  signifies the fluid friction entropy generation governance. As shown in Figure 9, with an increase of heating ratio, the contribution of heating in the total entropy generation value increases, and hence the Bejan Number increases. Moreover, an increase of aspect ratio in the influence of heating on total entropy generation rate per volume decreases. Physically, as the aspect ratio increases, the Rayleigh number is increased, the natural convection pumping power in the medium is improved, and stronger fluid circulation is observed. As a result, the irreversibility due to the fluid hydraulic resistance is also found to increase while the irreversibility due to the heat transfer drops.

Figure 10 demonstrates the role of heat source number in entropy generation. By observation of the total rate of entropy generation per volume (which is plotted against heating ratio for various numbers of heat sources at the open cavity), it is obvious that the number of heat sources is effective at high values of heating fluxes. The value of dimensionless entropy generation almost remains constant for the values  $\zeta < 10^{-1}$ , which reveals that the dimensionless irreversibility because of fluid and heat transfer is not changed meaningfully by an increase of input heat flux, while conduction heat transfer is the dominant mode of heat transfer in all parts of the cavity. By an increase of heat source number, that transition point moves to the lower heating ratios. Though the entropy generation by heat conduction declines by an increase in discrete heat source number, the value of dimensionless entropy generation increases by an increase in discrete heat source number after the transition heating ratio of the onset of natural convection and thermal radiation, since after  $\zeta = 1.3$  the entropy generated by the three discrete heat sources exceeds the entropy generated by the one discrete heat source. The rate of increase of

$S_{\text{total}}$  along with the magnitude of  $S_{\text{total}}$  is found to be the biggest for  $\zeta = 10$  for all the cases of the discrete heat source number. In optimizing thermal systems in open cavities it is necessary to minimize the entropy, so these onset values play crucial roles.



**Figure 9.** Bejan number for singular discrete heat sources as a function of heating ratio for various aspect ratios.



**Figure 10.** Dimensionless rate of total entropy generation for one and three discrete heat sources as a function of heating ratio.

Figure 11 demonstrates the role of number of heat sources on the heating portion of entropy generation. The Bejan number is plotted as a function of heating ratio for various numbers of heat sources at the open cavity; it is found that the number of heat sources is effective at high values of heating numbers. Since the number of discrete heat sources can increase both the fluid flow contribution and the heat transfer contribution in total entropy generation, the effect of number of discrete heat sources on Bejan number is not yet known. As demonstrated, at a low heating ratio the values for a single heater are higher than for three heaters, but at higher values the amount of total entropy generation rate per volume at the open cavity increases rapidly to the case of a single heater. By keen observation of the slope and manner of the curves of the Bejan number in Figure 11, the dominant contribution of fluid friction to entropy generation for different discrete heat source numbers at low values of dimensionless heat fluxes is revealed. As confirmed, at a low heating ratio the heating portion of entropy generation for a single heater is higher than for three heaters with a constant offset, but then at higher values the amount of the Bejan number for higher values of discrete heat sources will increase. It shows that the entropy generation due to heat transfer becomes more dominant with the augmentation of the heating ratio parameter.

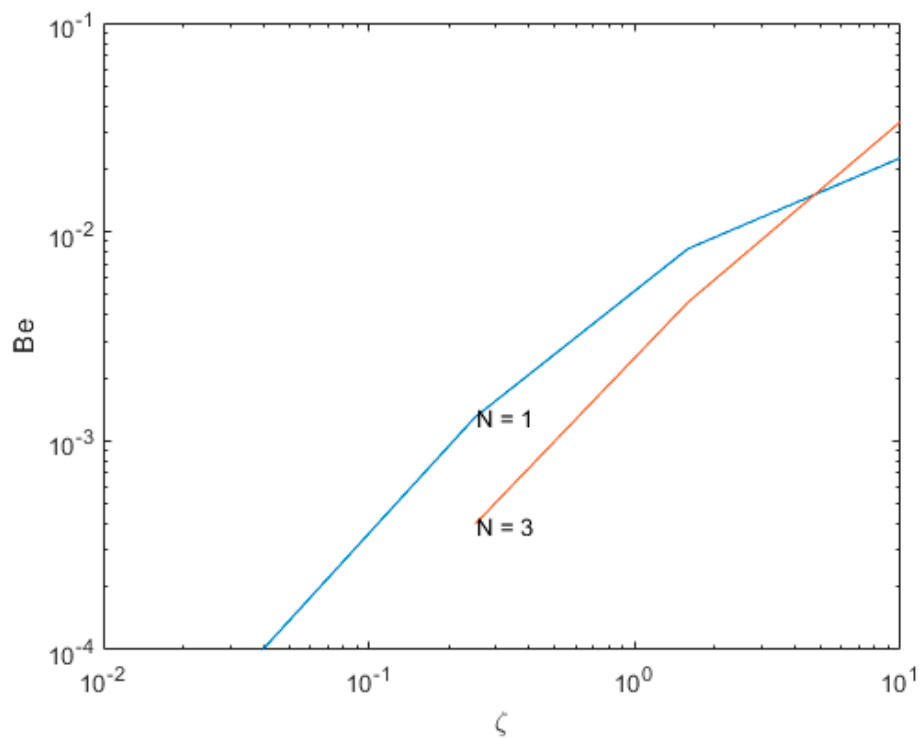


**Figure 11.** Bejan number for one and three discrete heat sources as a function of heating ratio.

#### 4. Conclusions

This paper presents the results of a detailed numerical investigation on thermal loading by radiant heaters in the presence of discrete heat sources. The second law of thermodynamics is considered to evaluate the energy quality management of thermal radiative heating, which plays a vital role in an enclosure. The governing Navier–Stokes equations of viscous fluid flow of conservation of mass, momentum, and energy (fluid and solid) are solved by the finite volume method and the SIMPLE algorithm. A parameter study is done based on the value of thermal load as well as an enclosure’s aspect ratio and the number of heaters. The results present the effect of thermal and geometrical parameters on entropy generation and an entropy distribution field. This limitation should be considered in the practical applications of the method and results of this paper. The results can be summarized as follows:

- (1) The entropy value was most influenced by temperature rather than density. The maximum values of entropy occur near the discrete heat sources despite the fact that the minimum values take place near the outlet and the top adiabatic plate. Most of the entropy generated by heat transfer was concentrated near the thermal boundary layer of the discrete heat sources.
- (2) The maximum friction entropy generation occurred in the right edge of the top plate and at the outlet boundaries of the cavity. The fluid friction declined with the augmentation of heat transfer at the bottom of the cavity.
- (3) The zone around the lamps contained the maximum values of entropy generation over the various parts of the enclosure.
- (4) It is clear that in most of the cavity the value of the Bejan number was less than 0.1, which proves that the dominant entropy generation was due to friction rather than heat transfer. Additionally, the highest values of Bejan numbers happen around the heat sources and near the bottom walls.
- (5) By an increase of heating ratio, the dimensionless entropy generation value remains constant at a low heating number and increases by an increase of heating number.
- (6) The increase of aspect ratio augments the dimensionless entropy generation rate per volume and the highest level of growth is observed at the entropy generation due to fluid friction.
- (7) The average Bejan number in the cavity rose with an increase of heating ratio. As shown by increase of heating ratio, the contribution of heating in the total entropy generation value increases. Furthermore, by the increase of aspect ratio, the contribution of irreversibility due to the heat transfer in total entropy generation rate per volume decreases.
- (8) By an increase of the heating ratio parameter, the irreversibilities due to the heat transfer enhances hugely in a higher scale compared to the entropy generation due to fluid friction.
- (9) The number of heat sources is effective at high values of heating fluxes. At a low heating ratio, the values for a single heater are higher than for three heaters, but at higher values the amount of total entropy generation rate per volume at the open cavity upsurges rapidly in the case of a single heater and the enhancement is more significant.
- (10) The number of heat sources is effective at high values of heating numbers. As well, at a low heating ratio, the heating portion of entropy generation for a single heater is higher than for three heaters with a constant offset (as the heat conduction mode is dominant), but then at higher values the amount of the Bejan number for higher values of discrete heat sources will increase.
- (11) The heating ratio of onset of natural and radiative entropy generation increases by an increase of number of discrete heat sources.

**Acknowledgments:** The last author acknowledges the support provided by FAPEMIG for this investigation. Truong Khang Nguyen would like to thanks TWAS (The World Academy of Science) for partially supporting of open access publishing (No. 16-184 RG\_PHYS\_AS\_I).

**Author Contributions:** Conceptualization, supervision, formal analysis, investigation, methodology, software, validation, visualization, writing the original draft, and editing is done by Mohammad Yaghoub Abdollahzadeh Jamalabadi. Project administration and Resources are provided by Mohammad Reza Safaei, Abdullah A.A.A. Al-Rashed, Truong Khang Nguyen and Enio Pedone Bandarra Filho. All authors have read and approved the final manuscript.

**Conflicts of Interest:** The authors declare no conflict of interest.

## Nomenclature

|          |   |
|----------|---|
| $A_R$    | Aspect ratio ( $H/L$ )                                  |
| $Be$     | Bejan number  |
| $Br$     | Brinkmann number  |
| $C_p$    | specific heat at constant pressure ( $J \cdot K^{-1}$ ) |
| $Gr$     | Grashof number ( $g\beta L^4 q''/\nu^2$ )               |
| $F_{ij}$ | Configuration factor                                    |
| $F_b$    | body force  |

|                           |   |
|---------------------------|---|
| $g$                       | acceleration due to gravity ( $\text{m}\cdot\text{s}^{-2}$ )            |
| $H$                       | Enclosure height (m)  |
| $k$                       | thermal conductivity ( $\text{W}\cdot\text{m}^{-1}\cdot\text{K}^{-1}$ ) |
| $L$                       | characteristic length (m)   |
| $n$                       | number of heat sources  |
| $N_r$                     | heating number ( $q''/\sigma T_\infty^4$ )                              |
| $N_s$                     | entropy generation number   |
| $Nu$                      | local Nusselt number  |
| $p$                       | pressure (Pa)   |
| $P$                       | dimensionless pressure ( $(p-p_\infty)L^2/\rho\alpha^2$ )               |
| $Pr$                      | Prandtl number ( $\nu/\alpha$ )   |
| $q''$                     | Heater heat flux ( $\text{W}\cdot\text{m}^{-2}$ )                       |
| $Ra$                      | Rayleigh number ( $g\beta L^4 q''/\nu\alpha$ )                          |
| $Re$                      | Reynolds number   |
| $S'''$                    | entropy generation rate per volume                                      |
| $S$                       | dimensionless entropy generation  |
| $S_\theta$                | dimensionless local entropy generation due to heat transport            |
| $S_\psi$                  | dimensionless local entropy generation due to fluid friction            |
| $S_{\theta,\text{total}}$ | dimensionless total entropy generation due to heat transport            |
| $S_{\psi,\text{total}}$   | dimensionless total entropy generation due to fluid friction            |
| $S_{\text{total}}$        | dimensionless total entropy generation due to heat and fluid friction   |
| $T$                       | temperature of the fluid (K)  |
| $T_h$                     | temperature of hot wall (K)   |
| $T_c$                     | temperature of cold wall (K)  |
| $U$                       | $x$ component of dimensionless velocity ( $v_x\cdot L/\alpha$ )         |
| $V$                       | $y$ component of dimensionless velocity ( $v_y\cdot L/\alpha$ )         |
| $\mathbf{v}$              | velocity vector   |
| $v_x$                     | $x$ component of velocity ( $\text{m}\cdot\text{s}^{-1}$ )              |
| $v_y$                     | $y$ component of velocity ( $\text{m}\cdot\text{s}^{-1}$ )              |
| $x$                       | distance along $x$ coordinate (m)                                       |
| $X$                       | dimensionless distance along $x$ coordinate ( $x/H$ )                   |
| $y$                       | distance along $y$ coordinate (m)                                       |
| $Y$                       | dimensionless distance along $y$ coordinate ( $y/H$ )                   |

### Greek Symbols

|               |   |
|---------------|---|
| $\alpha$      | thermal diffusivity ( $\text{m}^2\cdot\text{s}^{-1}$ )                |
| $\beta$       | volume expansion coefficient ( $\text{K}^{-1}$ )                      |
| $\delta_{ij}$ | Kronecker delta   |
| $\epsilon$    | surface emission factor   |
| $\theta$      | dimensionless temperature   |
| $\mu$         | dynamic viscosity ( $\text{kg}\cdot\text{m}^{-1}\cdot\text{s}^{-1}$ ) |
| $\rho$        | density ( $\text{kg}\cdot\text{m}^{-3}$ )                             |
| $\zeta$       | dimensionless heat flux ( $q''/\sigma T_\infty^4$ )                   |
| $\phi$        | viscous dissipation functions   |
| $\varphi$     | irreversibility distribution ratio                                    |
| $\psi_d$      | dimensional streamfunction ( $\text{m}^2\cdot\text{s}^{-1}$ )         |
| $\psi$        | dimensionless streamfunction  |

### Subscripts

|          |                                 |
|----------|---------------------------------|
| $\infty$ | bulk, ambient value             |
| $m$      | mean, modified, spatial average |
| $f$      | fluid                           |
| $eff$    | effective properties of fluid   |
| $s$      | solid                           |
| $total$  | summation over the domain       |

### Superscripts

|     |         |
|-----|---------|
| $e$ | element |
|-----|---------|

## References

- Bertrand, P.; Ignatiev, M.; Flamant, G.; Smurov, I. Pyrometry applications in thermal plasma processing. *Vacuum* **2000**, *56*, 71–76. [[CrossRef](#)]
- Ertem, M.E.; Sen, S.; Akar, G.; Pamukcu, C.; Gurgun, S. Energy balance analysis and energy saving opportunities for Erdemir slab furnace. *Energy Sources Part A Recovery Util. Environ. Eff.* **2010**, *32*, 979–994. [[CrossRef](#)]
- Jamalabadi, M.Y.A. Experimental investigation of thermal loading of a horizontal thin plate using infrared camera. *J. King Saud Univ. Eng. Sci.* **2014**, *26*, 159–167.
- Shimoda, H.; Sugano, A.; Watanabe, Y.; Kimura, T.; Ishiyama, K. Prediction method of unburnt carbon for coal fired utility boiler using image processing technique of combustion flame. *IEEE Trans. Energy Convers.* **1990**, *5*, 640–645. [[CrossRef](#)]
- Ben-Nasr, O.; Hadjadj, A.; Chaudhuri, A.; Shadloo, M.S. Assessment of subgrid-scale modeling for large-eddy simulation of a spatially-evolving compressible turbulent boundary layer. *Comput. Fluids* **2017**, *151*, 144–158. [[CrossRef](#)]
- Rashidi, M.M.; Nasiri, M.; Shadloo, M.S.; Yang, Z. Entropy generation in a circular tube heat exchanger using nanofluids: Effects of different modeling approaches. *Heat Transf. Eng.* **2017**, *38*, 853–866. [[CrossRef](#)]
- Alamian, R.; Shafaghat, R.; Shadloo, M.S.; Bayani, R.; Amouei, A.H. An empirical evaluation of the sea depth effects for various wave characteristics on the performance of a point absorber wave energy converter. *Ocean Eng.* **2017**, *137*, 13–21. [[CrossRef](#)]
- Ducoin, A.; Shadloo, M.S.; Roy, S. Direct Numerical Simulation of flow instabilities over Savonius style wind turbine blades. *Renew. Energy* **2017**, *105*, 374–385. [[CrossRef](#)]
- Sadeghi, R.; Shadloo, M.S. Three-dimensional numerical investigation of film boiling by the lattice Boltzmann method. *Numer. Heat Transf. Part A Appl.* **2017**, *71*, 560–574. [[CrossRef](#)]
- Sadeghi, R.; Shadloo, M.S.; Jamalabadi, M.Y.A.; Karimipour, A. A three-dimensional lattice Boltzmann model for numerical investigation of bubble growth in pool boiling. *Int. Commun. Heat Mass Transf.* **2016**, *79*, 58–66. [[CrossRef](#)]
- Sadeghi, R.; Shadloo, M.S.; Hooman, K. Numerical investigation of the natural convection film boiling around elliptical tubes. *Numer. Heat Transf. Part A Appl.* **2016**, *70*, 707–722. [[CrossRef](#)]
- Jamalabadi, M.Y.A. Joule heating in low-voltage electroosmotic with electrolyte containing nano-bubble mixtures through microchannel rectangular orifice. *Chem. Eng. Res. Des.* **2015**, *102*, 407–415. [[CrossRef](#)]
- Karimipour, A.; D'Orazio, A.; Shadloo, M.S. The effects of different nano particles of Al<sub>2</sub>O<sub>3</sub> and Ag on the MHD nano fluid flow and heat transfer in a microchannel including slip velocity and temperature jump. *Phys. E Low-Dimens. Syst. Nanostruct.* **2017**, *86*, 146–153. [[CrossRef](#)]
- Abdollahzadeh Jamalabadi, M.Y. Effects of micro-and macro-scale viscous dissipations with heat generation and local thermal non-equilibrium on thermal Developing forced convection in saturated porous media. *J. Porous Media* **2015**, *18*, 843–860. [[CrossRef](#)]
- Safaei, M.R.; Shadloo, M.S.; Goodarzi, M.S.; Hadjadj, A.; Goshayeshi, H.R. A survey on experimental and numerical studies of convection heat transfer of nanofluids inside closed conduits. *Adv. Mech. Eng.* **2016**, *8*, 7. [[CrossRef](#)]
- Shadloo, M.S.; Poultangari, R.; Jamalabadi, M.Y.A.; Rashidi, M.M. A new and efficient mechanism for spark ignition engines. *Energy Convers. Manag.* **2015**, *96*, 418–429. [[CrossRef](#)]
- Jamalabadi, M.Y.A.; Ghassemi, M.; Hamed, M.H. Two-dimensional simulation of thermal loading with horizontal heat sources. *Proc. Inst. Mech. Eng. Part C J. Mech. Eng. Sci.* **2012**, *226*, 1302–1308. [[CrossRef](#)]
- Abdollahzadeh Jamalabadi, M.Y.; Ghassemi, M.; Hamed, M.H. Numerical investigation of thermal radiation effects on open cavity with discrete heat sources. *Int. J. Numer. Methods Heat Fluid Flow* **2013**, *23*, 649–661. [[CrossRef](#)]
- Jamalabadi, M.Y.A. Effect of temperature dependent properties on thermal radiative loading of planar surfaces with distinct heaters. *J. Niger. Math. Soc.* **2016**, *35*, 159–177. [[CrossRef](#)]
- Harfash, A.J. Three dimensional simulations and stability analysis for convection induced by absorption of radiation. *Int. J. Numer. Methods Heat Fluid Flow* **2015**, *25*, 810–824. [[CrossRef](#)]
- Mehmet, O.; Mehmet Ali, C.; Hasancan, O.; Hüsnü, A.; Engin, B.; Tuba, C.; Özgür, I. CO<sub>2</sub> emission during the combustion of Orhaneli lignite coal. *World J. Eng.* **2017**, *14*, 27–34.



22. Das, D.; Basak, T. Role of distributed/discrete solar heaters for the entropy generation studies in the square and triangular cavities during natural convection. *Appl. Therm. Eng.* **2017**, *113*, 1514–1535. [[CrossRef](#)]
23. Salari, M.; Rezvani, A.; Mohammadtabar, A.; Mohammadtabar, M. Numerical study of entropy generation for natural convection in rectangular cavity with circular corners. *Heat Transf. Eng.* **2015**, *36*, 186–199. [[CrossRef](#)]
24. Doo, J.H.; Mun, G.S.; Ha, M.Y.; Seong, S.Y. Thermodynamic irreversibility induced by natural convection in square enclosure with inner cylinder. Part-II: Effect of vertical position of inner cylinder. *Int. J. Heat Mass Transf.* **2016**, *97*, 1120–1139. [[CrossRef](#)]
25. Kefayati, G.H.R. Heat transfer and entropy generation of natural convection on non-Newtonian nanofluids in a porous cavity. *Powder Technol.* **2016**, *299*, 127–149. [[CrossRef](#)]
26. Sheremet, M.A.; Oztop, H.F.; Pop, I.; Abu-Hamdeh, N. Analysis of entropy generation in natural convection of nanofluid inside a square cavity having hot solid block: Tiwari and Das' model. *Entropy* **2016**, *18*, 9. [[CrossRef](#)]
27. Chamkha, A.; Ismael, M.; Kasaeipoor, A.; Armaghani, T. Entropy generation and natural convection of CuO-Water nanofluid in C-shaped cavity under magnetic field. *Entropy* **2016**, *18*, 50. [[CrossRef](#)]
28. Selimefendigil, F.; Oztop, H.F.; Abu-Hamdeh, N. Natural convection and entropy generation in nanofluid filled entrapped trapezoidal cavities under the influence of magnetic field. *Entropy* **2016**, *18*, 43. [[CrossRef](#)]
29. Abdollahzadeh Jamalabadi, M.Y. Entropy generation in boundary layer flow of a micro polar fluid over a stretching sheet embedded in a highly absorbing medium. *Front. Heat Mass Transf.* **2015**, *6*, 1–13. [[CrossRef](#)]
30. Abdollahzadeh Jamalabadi, M.Y.; Hooshmand, P.; Bagheri, N.; KhakRah, H.; Dousti, M. Numerical simulation of Williamson combined natural and forced convective fluid flow between parallel vertical walls with slip effects and radiative heat transfer in a porous medium. *Entropy* **2016**, *18*, 147. [[CrossRef](#)]
31. Hooshmand, P.; Gatabi, H.R.; Bagheri, N.; Pirzadeh, I.; Hesabi, A.; Abdollahzadeh Jamalabadi, M.Y.; Oveisi, M. Numerical study of the magnetic field effects on the heat transfer and entropy generation aspects of a power law fluid over an axisymmetric stretching plate structure. *Entropy* **2017**, *19*, 94. [[CrossRef](#)]
32. Dixit, H.N.; Babu, V. Simulation of high Rayleigh number natural convection in a square cavity using the lattice Boltzmann method. *Int. J. Heat Mass Transf.* **2006**, *49*, 727–739. [[CrossRef](#)]
33. Vahl Davis, D.G. Natural convection of air in a square cavity: A benchmark solution. *Int. J. Numer. Methods Fluids* **1983**, *3*, 249–264. [[CrossRef](#)]
34. Shadloo, M.S.; Oger, G.; Touze, D.L. Smoothed particle hydrodynamics method for fluid flows, towards industrial applications: Motivations, current state, and challenges. *Comput. Fluids* **2016**, *136*, 11–34. [[CrossRef](#)]
35. Biswal, P.; Basak, T. Entropy generation vs energy efficiency for natural convection based energy flow in enclosures and various applications: A review. *Renew. Sustain. Energy Rev.* **2017**, *80*, 1412–1457. [[CrossRef](#)]
36. Oztop, H.F.; Kolsi, L.; Alghamdi, A.; Abu-Hamdeh, N.; Borjini, M.; Aissia, H.B. Numerical analysis of entropy generation due to natural convection in three-dimensional partially open enclosures. *J. Taiwan Inst. Chem. Eng.* **2017**, *75*, 131–140. [[CrossRef](#)]
37. Hussain, S.; Ahmed, S.E.; Akbar, T. Entropy generation analysis in MHD mixed convection of hybrid nanofluid in an open cavity with a horizontal channel containing an adiabatic obstacle. *Int. J. Heat Mass Transf.* **2017**, *114*, 1054–1066. [[CrossRef](#)]
38. Hinojosa, J.F.; David, B.; Xamán, J.; Pérez-Tello, M. The effect of surface thermal radiation on entropy generation in an open cavity with natural convection. *Int. Commun. Heat Mass Transf.* **2017**, *81*, 164–174. [[CrossRef](#)]

